Nanocomposites of polystyrene-*b*-polyisoprene copolymer with layered silicates and carbon nanotubes

Kiriaki Litina [a], Androniki Miriouni [a], Dimitrios Gournis [a,*],
Michael A. Karakassides [a], Nikolaos Georgiou [b], Emmanouel Klontzas [b],
Eleftherios Ntoukas [b], Apostolos Avgeropoulos [b,*]

[a] *Ceramics & Composites Laboratory, Department of Materials Science & Engineering, University of Ioannina, University Campus, 45110 Ioannina, Greece*
[b] *Polymers Laboratory, Department of Materials Science & Engineering, University of Ioannina, University Campus, 45110 Ioannina, Greece*

Abstract

Nanocomposites of polystyrene-*b*-polyisoprene (PS-*b*-PI) copolymer with layered-smectite clays (organically modified montmorillonite) and nanostructured clay-carbon nanotube hybrids were prepared. The diblock copolymer was synthesized by anionic polymerization using high-vacuum techniques and was molecularly characterized by size exclusion chromatography. Carbon nanotubes were developed on clay-supported nickel nanoparticles by the CCVD method. Nanotubes attached on the clay platelets were then chemically modified to create ester groups on their surfaces. PS-*b*-PI nanocomposites at various polymer to reinforcement loadings were prepared by solution intercalation. The final nanocomposites were characterized by powder X-ray diffraction, FT-IR spectroscopy, thermal analysis, and scanning electron microscopy. The experiments complemented with viscometry measurements reveal the successful incorporation of the reinforcements in the polymer mass.
© 2006 Elsevier Ltd. All rights reserved.

Keywords: Clay-polymer nanocomposites; Montmorillonite; Carbon nanotubes; Diblock copolymer; PS-*b*-PI

1. Introduction

In polymer nanocomposite research, the basic aim is to enhance several properties of polymeric components using molecular or nanoscale reinforcements. Polymers have been filled with several synthetic and/or natural compounds in order to increase tensile strength, modulus, heat resistance, impact resistance and electrical conductivity [1]. One area of research has focused on using layered-smectite clays as the reinforcing part of the matrix [1–3]. The presence of two dimensional platelike silicate layers in the matrix of a polymer was of major interest due to the significant gains in thermal

---

* Corresponding authors. Tel.: +30 26510 97366; fax: +30 26510 98690 (D. Gournis), tel.: +30 26510 97316; fax: +30 26510 97074 (A. Avgeropoulos).

E-mail addresses: dgourni@cc.uoi.gr (D. Gournis), aavger@cc.uoi.gr (A. Avgeropoulos).

stability [4], mechanical [5,6] and barrier properties of the resulting nanocomposites [7,8]. Depending on the strength of interfacial interactions between the polymer matrix and the layered silicate (modified or not), three different types of nanocomposites are thermodynamically achievable: (1) conventional composites, where packages of silicate layers, keep their stacking, creating a conventional phase separated composite (microcomposite), (2) intercalated nanocomposites, where the polymer chains are intercalated between the silicate layers, therefore increasing their gallery height but maintaining their layered stacking, resulting in a well ordered multi-layer with alternating polymer/silicate layers, (3) exfoliated nanocomposites, in which the individual clay layers lose their stacking and are exfoliated and dispersed in the continuous polymeric matrix [9]. Typical preparation methods of these nanocomposites include solution, melt intercalation, and in situ polymerization [9]. Solution intercalation has been very effective in incorporating exfoliated clays into polymers[10].

Equally promising reinforcement, for the creation of polymer nanocomposites, are carbon nanotubes. Since their discovery [11], carbon nanotubes (CNTs) have attracted unlimited attention due to their unique properties such as extremely high mechanical strength, high electrical and thermal conductivity [12,13]. This superior properties offer many opportunities for new composites. In this field of carbon nanotubes-based composites belong polymer/CNT composites, which combine exceptional mechanical, surface and multi-functional properties and strong interactions with the matrix resulting from the nano-scale microstructure and the large interfacial area [14,15]. However, CNTs are generally insoluble in common solvents and polymers, easy to agglomerate, bundle together and entangle, leading to many defect sites in the composites [16]. Several techniques have been applied to achieve homogeneous dispersion of CNTs in the polymer matrices such as: optimum physical blending, in situ polymerization and chemical functionalization [17]. Side-wall chemical functionalization is one of the most effective techniques for homogeneous dispersion of CNT in polymer matrices since strong interface adhesion is achieved between the functionalized carbon nanotubes and the surrounding polymer chains [18–22].

In addition, carbon nanotubes rooted on smectite layers are particularly attractive for polymer reinforcing applications. One would expect that the combined action of clay-carbon nanotubes in polymer matrixes would provide outstanding functionalities to the resulting composite materials. Towards this aim, Zhang et al. [23] demonstrated that the incorporation of CNT–clay hybrid system into nylon-6 by simple melt blending lead to exfoliated nanocomposites with excellent mechanical properties. Compared with neat polymer, the tensile modulus and the tensile strength of the composite were greatly improved, by about 290% and 150% respectively, by the incorporation of only 1 wt% CNT–clay hybrid reinforcement.

In the present study, we developed nanocomposites of polystyrene-b-polyisoprene with organically modified montmorillonite and hybrid systems of clays with functionalized carbon nanotubes at various polymer to reinforcement loadings. The block copolymer used in this research work was chosen to be a diblock copolymer of the PS-b-PI type, since such materials have been extensively studied and their molecular and morphological behavior is widely known [24,25]. The resulting nanocomposites were characterized by a combination of powder X-ray diffraction, FT-IR spectroscopy, thermal analysis, size exclusion chromatography, scanning electron microscopy, and viscometry measurements.

2. Experimental

2.1. Synthesis of diblock copolymer (PS-b-PI)

The diblock was prepared by anionic polymerization using high-vacuum techniques in evacuated, n-BuLi-washed, benzene-rinsed glass vessels. The purification of styrene (Merck), isoprene (Fluka), and benzene (Merck) to the standards required for anionic polymerization have been described elsewhere [26,27]. Additions were made through break seals and removals were accomplished through heat sealing of constrictions. sec-BuLi, prepared in vacuum from sec-butyl chloride and a lithium dispersion, was the initiator.

2.2. Organic modified clay (C_{16}-SWy)

The clay used in this work was a natural Wyoming montmorillonite (SWy-1) obtained from the Source Clay Minerals Repository, University of Missouri, Columbia with a cation-exchange capacity (CEC) of 76.4 meq/100 g clay. The clay was fractionated to <2 μm by gravity sedimentation and purified by standard methods in clay science [28].

Sodium-exchanged samples were prepared by immersing the clay into 1 N solution of sodium chloride. Cation-exchange was complete by washing and centrifuging four times with dilute solution of NaCl. The samples were finally washed with distilled-deionized water, transferred into dialysis tubes in order to obtain chloride free clays and then dried at room temperature.

To prepare the organoclay, a solution of the surfactant (hexadecyl-trimethyl ammonium bromide) in water (1.5 times the CEC of the clay) was added slowly to an aqueous 1 wt% clay suspension under vigorous stirring. The mixture was stirred for 24 h, centrifuged, washed with water three times, and air-dried by being spread on a glass-plate.

2.3. Clay/carbon nanotube hybrids (SWy-CNT-esters)

Suspension 1 wt% of montmorillonite was reacted with $NiCl_2 \cdot 6H_2O$ aqueous solution in order for the ratio of $[NiCl_2]/[clay]$ to be approximately 5. The solution was stirred for 3 h and then the clay-catalyst was rinsed repeatedly with distilled-deionized water, separated by centrifugation, dried at room temperature and finally calcined at 450 °C for 4.5 h. Carbon nanotubes were synthesized by catalytic decomposition of acetylene over Ni-clay in a fixed bed flow reactor at a temperature of 700 °C [29,30]. About 100 mg of the catalyst were placed in an alumina boat within a quartz tube, with an inner diameter of 2.2 cm and length of 90 cm, located in a resistance furnace. The sample was heated up to 700 °C at nitrogen atmosphere. At this temperature acetylene as a carbon precursor was admixed with the carrier gas (N_2) at a flow rate of 10 cm^3/min and 90 cm^3/min, respectively. Forty minute later, the C_2H_2 gas flow was stopped, and the ceramic boat was cooled down to room temperature in the nitrogen atmosphere. The deposited materials were finally collected from the ceramic boat.

The produced carbon nanotubes, developed on the clay surfaces, were functionalized as follows: 600 mg of clay/CNT were suspended in 80 ml of concentrated sulfuric acid/nitric acid mixture (3:1 (v/v)) and sonicated for 3 h. The suspension was then centrifuged and washed six times with water, in order to remove the excess of sulfuric and nitric acid, and dried at 50 °C in vacuum overnight. Sixty milligram of the purified nanotubes developed on clay surfaces, were sonicated in 90 ml of an aqueous

solution NaOH 10 mM for 2 min in order to be converted into the sodium salt form. Hundred milligram of tetra-n-octylammonium bromide (TOAB) and 1.5 mL of hexadecyl-bromide were added in the black homogeneous suspension and the mixture was refluxed at 80 °C for 4 h under vigorous stirring [18]. The precipitation was collected, resuspended in $CHCl_3$, centrifuged, washed with ethanol and dried at 50 °C in vacuum overnight.

2.4. Preparation of the nanocomposites

Diblock copolymer nanocomposites containing 1, 3, 5 and 7 wt% filler (organoclay or clay-CNT-esters) were prepared as follows: appropriate amount of the diblock copolymer was diluted in toluene (10 ml), and the solution was reacted with aliquots of the corresponding filler suspension in toluene as well (5 ml). The mixture was then stirred for 3 h, precipitated with methanol and air-dried by being spread on glass plates. Finally the solid samples were heated for 2 h under vacuum at 140 °C for the efficient removal of the solvent. The later was controlled with DSC measurements (not shown here).

2.5. Characterization

Size exclusion chromatography (SEC) experiments were carried out at 30 °C using a Spectra System PL 1000 pump, a Shodex RI 101 refractive index detector, and a Spectra System UV-1000 detector. Three mixed-C (Polymer Laboratories, with porous for efficient separation of molecules varying from 2000 to 4×10^6 g/mol) columns were used, thermo stated in a Lab Alliance column oven at 30 °C. THF, distilled over CaH_2 and sodium, was the carrier solvent at a flow rate of 1 mL/min. The X-ray powder diffraction data were collected on a D8 Advanced Bruker diffractometer by using CuK_a (40 kV, 40 mA) radiation and a secondary beam graphite monochromator. The patterns were recorded in a 2θ range from 2° to 40°, in steps of 0.02° and counting time 2 s per step. Infrared spectra were measured with a FT-IR 8400 spectrometer, in the region of 400–4000 cm^{-1}, equipped with a DTGS detector. Each spectrum was the average of 32 scans collected at 2 cm^{-1} resolution. Samples were in the form of KBr pellets containing ca. 2 wt% sample. Thermogravimetric (TGA) and differential thermal (DTA) analysis were performed using a Perkin Elmer Pyris Diamond TG/DTA.

Samples of approximately 5 mg were heated in air from 25 to 850 °C, at a rate of 5 °C/min. Scanning electron images were recorded using a JEOL JSM-5600V scanning electron microscope (SEM). The samples were coated with a thin film of conducting metal (Au) to avoid charge problems at the pictures. The images are typical and representative of the samples under observation. The viscometry measurements were accomplished by using a type 0c Ubbelohde suspended level dilution viscometer (suitable only for toluene) at a thermo stated water bath of 35 °C. Toluene is a common good solvent for both segments of the copolymer. The solvent was refluxed over CaH_2 for 24 h and was fractionally distilled prior to use.

3. Results and discussion

The diblock copolymer was synthesized with anionic polymerization techniques using sequential addition of the monomers in the solvent under high-vacuum. The reactions used are shown in Scheme 1. The major advantage of the sequential addition of monomers is that the final copolymer is synthesized quickly, when compared with other synthesis approaches (e.g., linking reaction of the two different chains), without any side-reactions and with narrow polydispersity indices ($I < 1.1$). The precursor (PS) and the final diblock copolymer (PS-b-PI) were monitored via SEC in order to distinguish the polydispersity index I ($I = \overline{M}_w/\overline{M}_n$, $\overline{M}_w$ is the average molecular weight per weight and $\overline{M}_n$ is the average molecular weight per number) of both polymers (Fig. 1). From the graphs differential refractive index (DRI) vs. elution volume, it is clearly understood that both macromolecules are model, thus exhibit compositional and molecular homogeneity [27]. It is clearly understood from
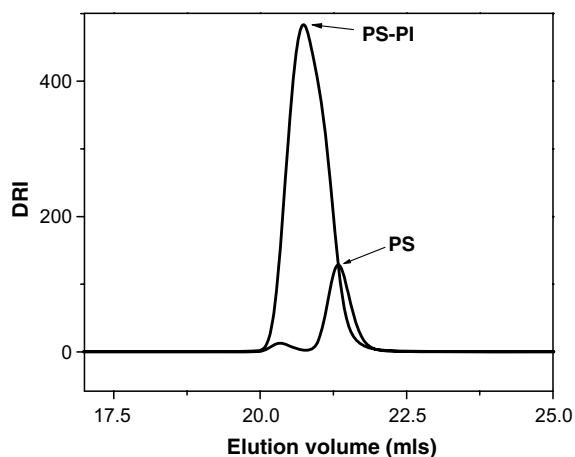
Fig. 1. Differential refractive index vs. elution volume for the precursor (PS) and the final diblock copolymer (PS-b-PI).

Table 1
Results from size exclusion chromatography

Sample	$\overline{M}_w$ ($\times 10^{-3}$ g/mol)	$\overline{M}_n$ ($\times 10^{-3}$ g/mol)	I
PS	29.3	28.9	1.014
PS-b-PI	38.2	36.9	1.035

Fig. 1 that the SEC graph of the PS block is bimodal, as a result of the unsuccessful termination of the living $PS^{(-)}Li^{(+)}$ ends, due to the fact that MeOH (termination reagent) was not well degassed. The dimer peak is approximately ~3% of the whole chromatograph [27]. The molecular characterization results are exhibited in Table 1. The weight fraction is 0.78 for PS and 0.22 for PI, values that lead to hexagonally closed packed cylindrical domains of PI in a PS matrix if morphological characterization occurs via transmission electron microscopy (TEM) and small angle X-ray scattering techniques (SAXS). Such results are already reported in the literature [24] for linear diblock copolymers in the weak segregation regime (low molecular weight copolymer leading to $\chi N \sim 28$, where χ is the Flory–Huggins interaction parameter between the two different segments [25] and N is the degree of polymerization for the copolymer).

Evidence for the successful bonding of alkylated ester groups to the surfaces of CNTs, in the clay-CNT composite, is provided by thermal defunctionalization results [31,32]. Thermal defunctionalization is based on the observation that the necessary temperature for elimination of functional groups bound to nanotubes is considerably lower than for the nanotube itself, enabling in this way
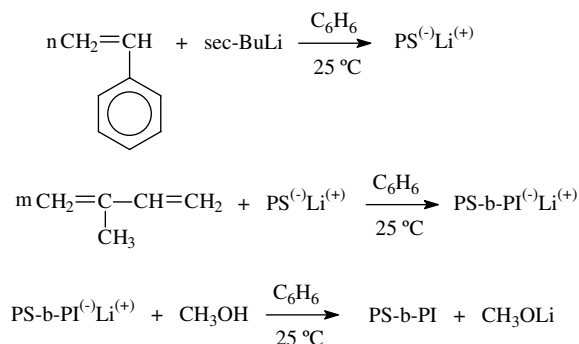
Scheme 1. Synthetic pathway of the diblock copolymer.

selective removal of the functional groups in a thermal analysis scan. Fig. 2 shows the DTA–TG curves, under air, of the SWy-CNT composite before and after the chemical functionalization. Clay/carbon nanotubes, before the functionalization, show only one exothermic peak at 620 °C due to the oxidation (destruction) of the nanotubes [33]. From the weight loss in the TGA curve it is calculated that the carbon nanotubes correspond to about 45 wt% of the total mass while in the purified-functionalized sample the CNT content is lower (∼30–35 wt%). After the chemical modification and the creation of ester groups on the surface of the nanotubes this

exothermic peak is shifted at lower temperature (576 °C), providing evidence for the successful chemical functionalization. The second exothermic peak (at 303 °C), in the diagram of SWy-CNT-esters, could be attributed to the loss of aliphatic ester groups bonded to nanotubes. The weight loss due to aliphatic groups can be estimated to about 10 wt%, giving an approximate degree of functionalization.

The intercalation capability of the diblock copolymer PS-*b*-PI was evaluated by XRD measurements. A series of XRD patterns recorded from: the sodium-montmorillonite (SWy), the organoclay (C$_{16}$-SWy), the diblock copolymer (PS-*b*-PI) and
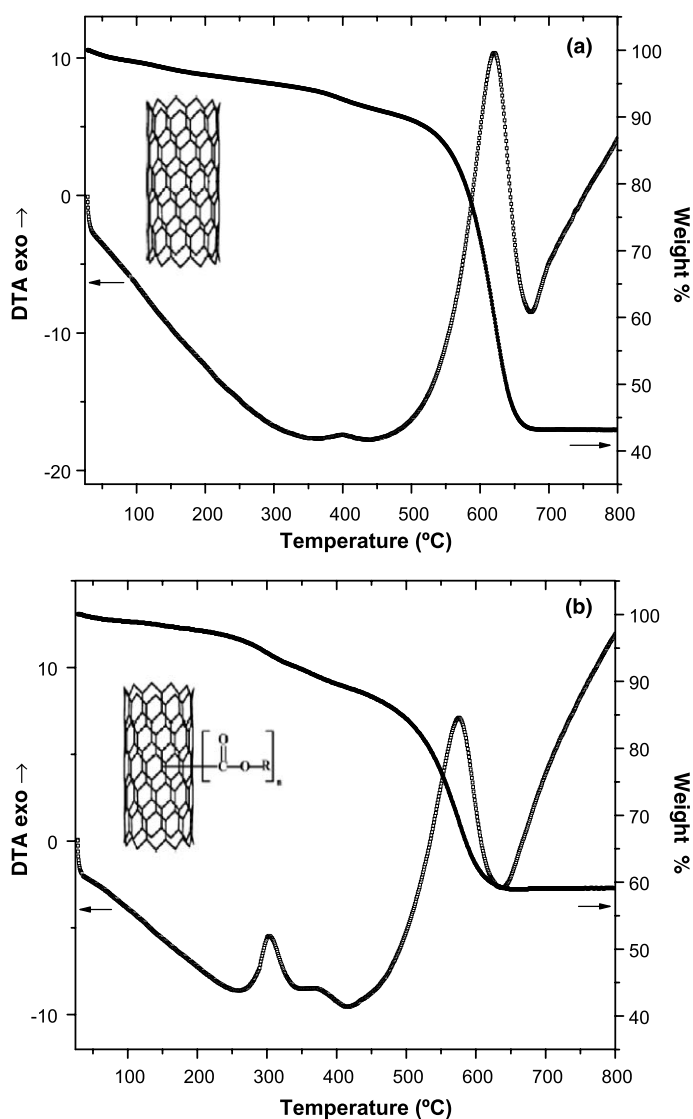
Fig. 2. TGA and DTA curves of (a) SWy-CNT and (b) SWy-CNT-esters.
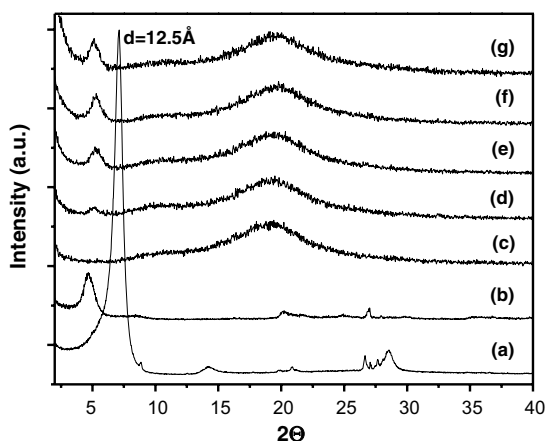
Fig. 3. XRD patterns of (a) SWy, (b) C_{16}-SWy, (c) PS-*b*-PI and nanocomposites with C_{16}-SWy at different wt% loadings, (d) 1%, (e) 3%, (f) 5% and (g) 7%.

Fig. 4. XRD patterns of (a) Ni-SWy, (b) purified CNTs, (c) SWy-CNT-esters, (d) PS-*b*-PI and nanocomposites with SWy-CNT-esters at different wt% loadings, (e) 1%, (f) 3%, (g) 5% and (h) 7%.

the hybrid systems PS-*b*-PI/1% C_{16}-SWy, PS-*b*-PI/3% C_{16}-SWy, PS-*b*-PI/5% C_{16}-SWy and PS-*b*-PI/7% C_{16}-SWy are shown in Fig. 3. An increase of the basal spacing (d_{001}) of the clay mineral is observed after the insertion of the organic surfactant. More specifically, the pristine Na-montmorillonite shows a d_{001}-spacing of 12.5 Å which correspond to an intersheet space $\Delta = 12.5 - 9.6 = 2.9$ Å, where 9.6 Å is the thickness of the clay layer, in the case of organo-modified clay, the basal spacing d_{001} becomes 18.8 Å, due to an intersheet separation of $18.8 - 9.6 = 9.2$ Å. This 9.2 Å distance of the organoclay arises from a conformation where the organic chains are inclined (at a certain angle) to the surface. The nearly constant d_{001} values at 16.9, 16.9, 16.7 and 17.28 Å for the PS-*b*-PI nanocomposites loaded with 1, 3, 5 and 7 wt% C_{16}-SWy respectively indicates a considerable decrease in the d_{001} distance of the organoclay (the wide peak at $2\Theta = 19.2°$ comes from the copolymer). The decrement in the d_{001}-spacing after mixing with the polymeric mass may be attributed to a decrease in the mobility of the long carbon chain of the surfactant with a concomitant reduction from their arrangements in the clay layers. The presence of d_{001} peak in the XRD patterns of the nanocomposites indicates probably the formation of intercalated structures, where the organically modified silicate layers are kept in order with a new part of the PS-*b*-PI chains to be hosted in the clay galleries, while the major amount of these surround the silicate layers. The viscometry results (see below) gave additional evidence for the existence of these intercalated hybrid structures.

Fig. 4 shows the XRD patterns of the parent materials and the copolymer nanocomposites with the clay-CNT-esters in different loadings. The diffraction pattern of Ni-montmorillonite-450 °C shows a peak at $2\Theta = 9.25°$, which correspond to d_{001}-spacing of Ni-montmorillonite after calcination in air. In the same pattern the presence of nickel-oxides originating from the exchangeable metal cations, during thermal treatment, is also observed. After the CCVD process for the production of CNTs the XRD pattern shows the appearance of a new peak at $2\Theta = 26.4°$, which correspond to the 002 reflection of graphite structure and reveals the successful production of CNTs [34]. The same peak is also observed in the pattern of clay-CNT sample after the chemical functionalization. The existence of this reflection in the diffraction patterns of all polymer nanocomposites clearly proves the appearance of CNTs in the final polymeric composites. On the other hand, the absence of the d_{001} diffraction peak, characteristic of the Ni-clay, in the patterns of the final nanocomposites indicates that the ordered structure of the layered mineral is effectively eliminated after mixing with the polymeric mass. A schematic illustration showing the procedure of growing CNTs on Ni-clay, the purification and chemical functionalization step and finally the incorporation of clay-CNT-esters into PS-*b*-PI polymer is presented in Scheme 2.

Fig. 5 shows the FT-IR spectra of the nanocomposite PS-*b*-PI/5% C_{16}-SWy, in comparison with the pristine clay, organoclay and the neat copolymer. The spectrum of the PS-*b*-PI/5% C_{16}-SWy hybrid presents all the characteristic bands of the

copolymer PS-*b*-PI and of the organo-montmoril-
lonite, without significant changes, confirming the
presence of the organoclay mineral in the final nano-
composite. The appearance of the peaks at 466 and
1036 cm^{-1} which correspond to Si–O and Si–O–Si
vibrations of the clay lattice are indicative of the
existence of the phyllomorphous mineral in the final
composite. Similar spectra were observed for all the
series of nanocomposites (not shown here).

The mean radius of gyration [35] for polymers of
known molecular weight can be approximately cal-
culated by using the method of viscometry for dilute
solutions. In this method through the determination
of the intrinsic viscosity of the polymer, the calcula-
tion of the radius of gyration is possible. The flow
time of the solvent (t_0) and the polymer (t_i) in the
viscometer under stable temperature, in various
concentrations is being measured. Through the flow
time the relative viscosity (η_r) and the specific viscos-
ity (η_{sp}) are determined from Eqs. (1) and (2) respec-
tively, which are indicated below:

$$\eta_r = t_i/t_0 \tag{1}$$
$$\eta_{sp} = (t_i - t_0)/t_0 = \eta_r - 1 \tag{2}$$

Using Huggins and Kraemer equations, as exhibited
in relations (3) and (4) respectively, the plots of η_{sp}/C
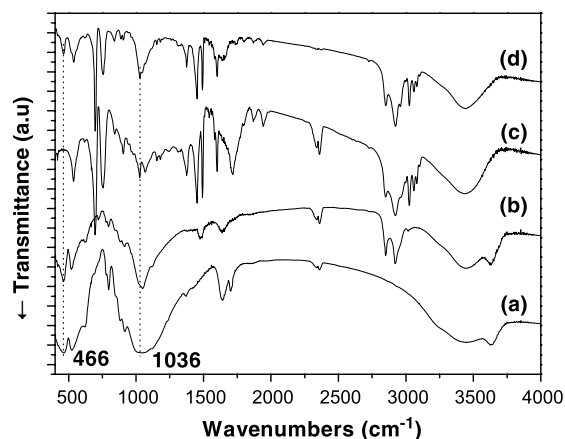
Fig. 5. FT-IR spectra of (a) SWy, (b) C$_{16}$-SWy, (c) PS-*b*-PI and
(d) nanocomposite with 5 wt% C$_{16}$-SWy.

and ln η_r/C vs. polymer concentration (C) can be ob-
tained. From the mutual extrapolation to infinite
dilution ($C \to 0$) of both equations the intrinsic vis-
cosity, [η], can be calculated.

$$\eta_{sp}/C = [\eta] + K_H[\eta]^2 C \tag{3}$$
$$\ln \eta_r/C = [\eta] + K_C[\eta]^2 C \tag{4}$$
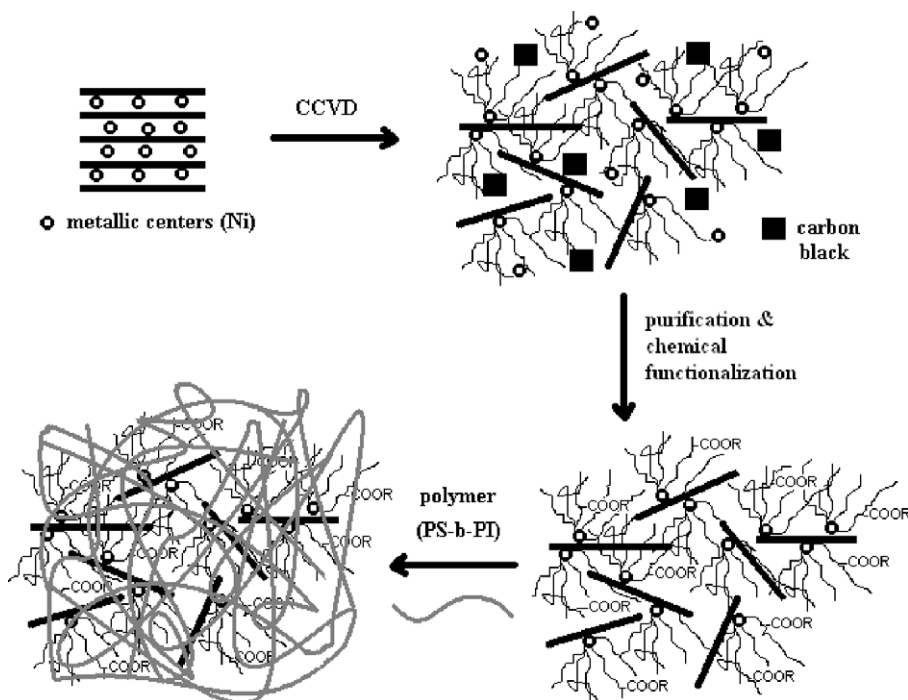
Scheme 2. Schematic illustration of the synthetic steps used for the preparation of the PS-*b*-PI/clay-CNT-esters nanocomposites.

Finally by using Flory's equation (5) the polymer's radius of gyration is calculated. $[\eta]$ is the intrinsic viscosity, $\overline{M}_w$ is the average molecular weight per weight of the PS-*b*-PI copolymer and Φ is Flory's constant and equal to 2.5×10^{21} when $[\eta]$ is given in dL/g units and does not differ for the two different components, as is the case for PS and PI polymeric chains. From the literature [36–39] values for intrinsic viscosities and mean radius of gyration can be provided for both homopolymers of PS and PI.

$$\langle \overline{S}^2 \rangle^{3/2} = \frac{[\eta]M_w}{\Phi} \qquad (5)$$

In Table 2 results are given for the intrinsic viscosity $[\eta]$ (in mL/g units) and the mean radius of gyration $\langle S^2 \rangle^{1/2}$ (in nm), respectively, by using the aforementioned relations for the neat copolymer, and various composites of the copolymer with 1 wt% C_{16}-SWy and 1 wt% SWy-CNT-esters. From Table 2 results it is obvious that the mean radius of gyration is being minimized if the copolymer is in a 99:1 ratio with various low dimensional materials when compared to the neat copolymer's value. This behavior can be explained if one considers that the polymeric chains are being skewed when the layered material is added therefore decreasing the distance from the periphery of the macromolecular entanglements, a behavior which lowers the value of the mean radius of gyration. Thus the copolymer behaves in the solution almost like a theta solvent is being used despite the fact that toluene is a good non-selective solvent for both segments. Especially in the case when C_{16}-SWy (organoclay) is being added major decreases are observed in the $[\eta]$ and $\langle S^2 \rangle^{1/2}$ values. Possibly some of the polymer chains are distributed inside the layers of the organophilic materials therefore enhancing the flow and decreasing the flow time in the viscometer. The decrease is almost distinct in the case when SWy-CNT-esters are being used. Therefore the SWy-CNT-esters are being distributed inside the polymer solution without affecting distinctively the viscometric properties of the copolymers. Such behavior leads to the conclusion that the SWy-CNT-esters additions are not altering the flow of the copolymer but only in a very small manner, leading to well distributed ceramic materials inside the entanglements of the polymeric chains.

The uniform dispersion of the clay/CNTs composites in the polymer mass was further revealed using scanning electron microscopy. Fig. 6(A) shows the SEM image of the carbon nanotubes, embedded on the clay surface, which were first

Table 2
Results of the intrinsic viscosity $[\eta]$ (in mL/g) and the mean radius of gyration $\langle S^2 \rangle^{1/2}$ (in nm)

Sample	$[\eta]$ (mL/g)	$\langle S^2 \rangle^{1/2}$ (nm)
Neat PS-*b*-PI	32.2	15.692
PS-*b*-PI/1% C_{16}-SWy	17.8	12.878
PS-*b*-PI/1% SWy-CNT-esters	31.7	15.610
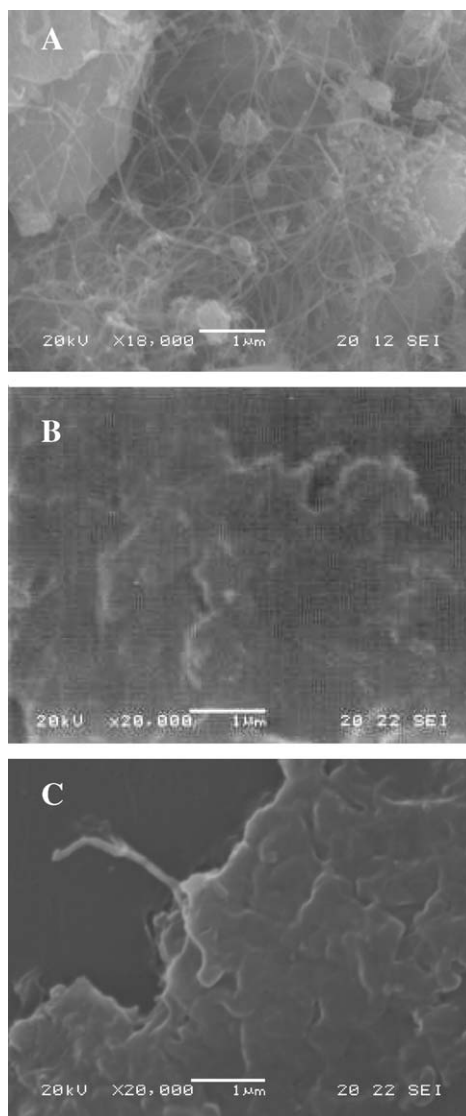
Fig. 6. (A) Typical SEM image showing the morphology of MWNTs, (B) SEM image showing an overall morphology of surface for PS-*b*-PI nanocomposite containing 3 wt% SWy-CNT-esters and (C) the same nanocomposite after tensile test showing a nanotube which is stretched out of the polymer surface.

purified and then treated with TOAB and hexade-cyl-bromide, as described above. The tubes are randomly entangled together on the surface of the clay mineral. Fig. 6(B) exhibits the surface of the nanocomposite, which contains 3 wt% SWy-CNT-esters. Homogeneous dispersion of the reinforcement throughout the polymer matrix is being observed. The fracture surface of the nanocomposite after applying a tensile force is shown in Fig. 6(C). This image indicates that upon failure the nanotubes are broken rather than just pulled out of the polymer matrix. More specifically, a nanotube is observed to be stretched out of the polymer surface with a curved end, while the other end is still embedded in the matrix. This phenomenon of the CNTs upon tensile stretching proves a strong interfacial adhesion between CNTs and the PS-*b*-PI matrix. Similar results were reported from Zhang et al. [22] on carbon nanotubes reinforced nylon-6 composite prepared by simple melt-compounding. Further work is in progress concerning the mechanical properties and the microscopic characterization of the nanocomposites.

4. Conclusion

In summary, we have investigated the insertion of two reinforcements: C_{16}-SWy and SWy-CNT-esters, in various percentages, into a diblock copolymer PS-*b*-PI and the subsequent behavior of the nanocomposites. XRD measurements showed that in the case of SWy-CNT-esters exfoliated nanocomposites were obtained, while the addition of C_{16}-SWy leads to intercalated structures. FT-IR and viscometry measurements confirmed the presence of the reinforcements in the final composite materials while SEC and thermal analysis were used to examine the successful synthesis of the copolymer and the functionalized nanotubes, respectively. Finally SEM experiments showed the morphology of clay-carbon nanotubes and the strong interfacial adhesion between CNTs and the PS-*b*-PI chains.

Acknowledgments

References

[1] Kojima Y, Usuki A, Kawasumi M, Okada A, Kurauchi T, Kamigaito O. Synthesis of nylon-6-clay hybrid by montmorillonite intercalated with epsilon-caprolactam. J Polym Sci Part A: Polym Chem 1993;31(4):983–6.

[2] Jacob MME, Hackett E, Giannelis EP. From nanocomposite to nanogel polymer electrolytes. J Mater Chem 2003; 13(1):1–5.

[3] Gournis D, Floudas G. "Hairy" plates: poly(ethylene oxide)-*b*-polyisoprene copolymers in the presence of laponite clay. Chem Mater 2004;16(9):1686–92.

[4] Blumstein A. Polymerization of adsorbed monolayer. II. Thermal degradation of the inserted polymer. J Polym Sci A 1965;3(7):2665–72.

[5] Kojima Y, Usuki A, Kawasumi M, Okada A, Kurauchi T, Kamigaito O. One-pot synthesis of nylon-6 clay hybrid. J Polym Sci Part A: Polym Chem 1993;31(7):1755–8.

[6] Ray SS, Yamada K, Okamoto M, Ueda K. New polylactide-layered silicate nanocomposites. 2. Concurrent improvements of material properties, biodegradability and melt rheology. Polymer 2003;44(3):857–66.

[7] Giannelis EP. Polymer layered silicate nanocomposites. Adv Mater 1996;8(1):29–35.

[8] LeBaron PC, Wang Z, Pinnavaia TJ. Polymer-layered silicate nanocomposites: an overview. Appl Clay Sci 1999; 15(1–2):11–29.

[9] Ray SS, Okamoto M. Polymer/layered silicate nanocomposites: a review from preparation to processing. Prog Polym Sci 2003;28(11):1539–641.

[10] Pinnavaia TJ, Beall GW. Polymer-clay nanocomposites. New York: John Wiley & Sons; 2001.

[11] Iijima S. Helical microtubules of graphitic carbon. Nature 1991;354(6348):56–8.

[12] Baughman RH, Zakhidov AA, de Heer WA. Carbon nanotubes – the route toward applications. Science 2002;297(5582):787–92.

[13] Ajayan PM. Nanotubes from carbon. Chem Rev 1999; 99(7):1787–99.

[14] Li YL, Kinloch IA, Windle AH. Direct spinning of carbon nanotube fibers from chemical vapor deposition synthesis. Science 2004;304(5668):276–8.

[15] Dalton AB, Collins S, Munoz E, Razal JM, Ebron VH, Ferraris JP, et al. Super-tough carbon-nanotube fibres – these extraordinary composite fibres can be woven into electronic textiles. Nature 2003;423(6941):703.

[16] Qian D, Dickey EC, Andrews R, Rantell T. Load transfer and deformation mechanisms in carbon nanotube-polystyrene composites. Appl Phys Lett 2000;76(20): 2868–70.

[17] Xie XL, Mai YW, Zhou XP. Dispersion and alignment of carbon nanotubes in polymer matrix: a review. Mater Sci Eng R-Rep 2005;49(4):89–112.

[18] Li SP, Qin YJ, Shi JH, Guo ZX, Yongfang L, Zhu DB. Electrical properties of soluble carbon nanotube/polymer composite films. Chem Mater 2005;17(1):130–5.

[19] Lin Y, Zhou B, Fernando KAS, Liu P, Allard LF, Sun YP. Polymeric carbon nanocomposites from carbon nanotubes functionalized with matrix polymer. Macromolecules 2003; 36(19):7199–204.

[20] Viswanathan G, Chakrapani N, Yang HC, Wei BQ, Chung HS, Cho KW, et al. Single-step in situ synthesis of

polymer-grafted single-wall nanotube composites. J Am Chem Soc 2003;125(31):9258–9.

[21] Qin SH, Oin DQ, Ford WT, Resasco DE, Herrera JE. Polymer brushes on single-walled carbon nanotubes by atom transfer radical polymerization of n-butyl methacrylate. J Am Chem Soc 2004;126(1):170–6.

[22] Zhang WD, Shen L, Phang IY, Liu T. Carbon nanotubes reinforced nylon-6 composite prepared by simple melt-compounding. Macromolecules 2004;37(2):256–9.

[23] Zhang WD, Phang IY, Liu TX. Growth of carbon nanotubes on clay: unique nanostructured filler for high-performance polymer nanocomposites. Adv Mater 2006; 18(1):73–7.

[24] Avgeropoulos A, Dair BJ, Thomas EL, Hadjichristidis N. Swelling behavior of ordered miktoarm star block copolymer-homopolymer blends. Polymer 2002;43(11):3257–66.

[25] Owens JN, Gancarz IS, Koberstein JT, Russell TP. Investigation of the microphase separation transition in low-molecular weight diblock copolymers. Macromolecules 1989;22(8):3380–7.

[26] Morton M, Fetters LJ. Rubber Chem Technol 1975;48: 359.

[27] Iatrou H, Hadjichristidis N. Synthesis of a model 3-miktoarm star terpolymer. Macromolecules 1992;25(18):4649–51.

[28] King RD, Nocera DG, Pinnavaia TJ. On the nature of electroactive sites in clay-modified electrodes. J Electroanal Chem 1987;236(1–2):43–53.

[29] Gournis D, Karakassides MA, Bakas T, Boukos N, Petridis D. Catalytic synthesis of carbon nanotubes on clay minerals. Carbon 2002;40(14):2641–6.

[30] Jankovic L, Gournis D, Dimos K, Karakassides MA, Bakas T. Catalytic production of carbon nanotubes over first row transition metal oxides supported on montmorillonite. J Phys: Conf Ser 2005;10(1):178–81.

[31] Georgakilas V, Gournis D, Karakassides MA, Bakandritsos A, Petridis D. Organic derivatization of single-walled carbon nanotubes by clays and intercalated derivatives. Carbon 2004;42(4):865–70.

[32] Saini RK, Chiang IW, Peng HQ, Smalley RE, Billups WE, Hauge RH, et al. Covalent sidewall functionalization of single wall carbon nanotubes. J Am Chem Soc 2003;125(12):3617–21.

[33] Shi ZJ, Lian YF, Liao FH, Zhou XH, Gu ZN, Zhang YG, et al. Purification of single-wall carbon nanotubes. Solid State Commun 1999;112(1):35–7.

[34] Zhu WZ, Miser DE, Chan WG, Hajaligol MR. Characterization of multiwalled carbon nanotubes prepared by carbon arc cathode deposit. Mater Chem Phys 2003;82(3):638–47.

[35] Cowie JMG. Polymers: Chemistry & Physics of modern materials. London: Blackie Academic & Professional; 1997.

[36] Pispas S, Avgeropoulos A, Hadjichristidis N, Roovers J. Hydrodynamic properties of A(8)B(8) type miktoarm (Vergina) stars. J Polym Sci Part B: Polym Phys 1999; 37(12):1329–35.

[37] Prudhomm J, Bywater S, Roovers JEL. Solution properties of isoprene-styrene block copolymers. Eur Polym J 1972;8(7):901–10.

[38] Roovers JEL, Bywater S. Preparation and characterization of 4-branched star polystyrene. Macromolecules 1972; 5(4):384–8.

[39] Hadjichristidis N, Roovers JEL. Synthesis and solution properties of linear, 4-branched, and 6- branched star polyisoprenes. J Polym Sci Part B: Polym Phys 1974; 12(12):2521–33.